ACS OMEGA

Open Access

http://pubs.acs.org/journal/acsodf

Article

Controllable Synthesis of Hollow Silica Nanoparticles Using Layered Double Hydroxide Templates and Application for Thermal Insulation Coating

Minh Vuong Phan,* Thi Kim Thoa Tran, Quynh Nhu Pham, Manh Huy Do, Thi Hong No Nguyen, Minh Ty Nguyen, Thanh Thao Phan, and Thi Xuan Hang To

Cite This: *ACS Omega* 2023, 8, 31399−31409

Read Online

ACCESS | Metrics & More | Article Recommendations | Supporting Information

ABSTRACT: The innovative hollow silica nanoparticle (HSN) material possesses substantial potential for application in the insulation field. The size and shell thickness of HSN are crucial factors in determining their inherent properties, which, in turn, impact their applicability. This research presents a facile approach to synthesizing HSN in which sodium silicate (Na_2SiO_3) was utilized as the silica precursor that can be directly deposited onto layered double hydroxide (LDH) nanoparticles without the utilization of any surfactant. A subsequent acid treatment was used to eliminate the templates, resulting in the formation of an HSN devoid of mesopores in silica shells. By utilizing various sizes of LDH cores, obtainable via coprecipitation followed by hydrothermal treatment, we were capable of successfully synthesizing the hollow particles with adjustable diameters ranging from 50 to 200 nm. In addition, the shell thickness is varied from 6.8 to 22.5 nm by varying the silicate solution concentration. Results demonstrate that prepared HSNs have low thermal conductivity and high reflectance in the UV−vis−NIR range (averaging 82.1%). These findings suggest that HSN can be utilized as an effective inorganic filler in the formulation of reflective and thermally insulating coatings.

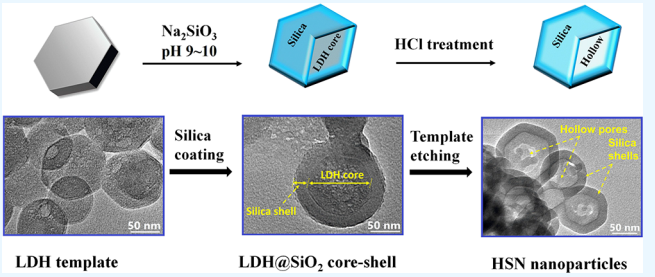

1. INTRODUCTION

Hollow silica nanoparticles (HSN) have gained significant interest from scientists owing to their unique properties, such as low density, thermal stability, and chemically inertness.[1,2] Silica is nontoxic and easier to disperse in polymers than other fillers. This makes it become a secure option and a prospective candidate for the advancement of a variety of fields, including catalysis,[3−5] drug delivery,[6−9] biomedical application,[10] optical materials,[11,12] and especially thermal insulation materials.[13−15]

While assuming only air exists inside the hollow pores, they can interrupt the heat transfer from the environment through the material and reduce thermal conductivity.[16,17] Silica shells without mesopore channels revealed some important properties of the HSN materials. Their solid shell can separate the hollow pore interior from the outer medium and prevent the adsorption, mass transfer, or penetration of molecules into or out of the gas pores.[18,19] This significantly influences the product properties, such as density, thermal conductivity, refractive index, or permittivity, especially when they are incorporated into the polymer matrix.[2,20] Indeed, epoxy resin was found to be filled into the hollow core of HSN through the mesopore on the silica shells, which affects the low-permittivity characteristic of the epoxy composite.[2,20] The SiO_2 shell also exhibits remarkable light reflection properties, which are influenced by shell thickness.[21,22] It could be noticed that particle size and shell thickness are also critical factors that influence the characteristics of HSN.[13,17,22] As a result, researchers have focused on controlling these characteristics to provide a versatile platform with a diverse array of potential applications.

One of the most widespread methods for synthesizing HSN involves covering a polystyrene (PS) template with tetraethyl orthosilicate (TEOS) based on the modified Stöber process, then removing the template through calcination or dissolution.[23−27] The surface-active agents are also employed to alter the surface characteristics of the polymer template, thereby increasing the variety of positively charged sites that facilitate the association of silica precursors on the template surface.[27] This method enables the production of HSN with controlled morphology, particle size, and shell thickness. However, applying additives to improve the coating efficiency results in forming a mesoporous channel in the shell, which decreases

Received: June 4, 2023
Accepted: August 3, 2023
Published: August 17, 2023

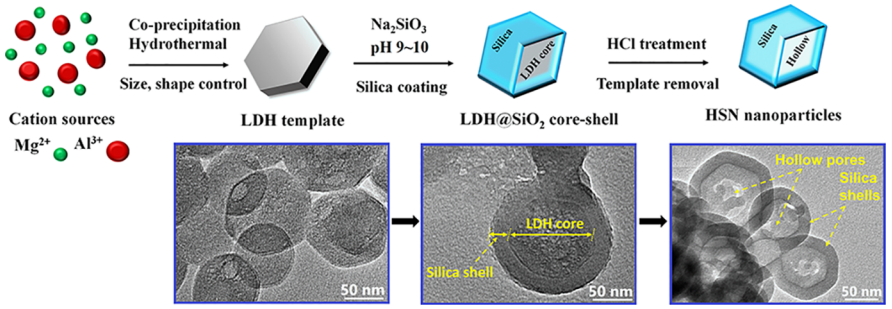

Figure 1. (Top) Schematic illustration of the fabrication of hollow silica. (Bottom) Corresponding TEM images of the prepared particles at each stage of the process.

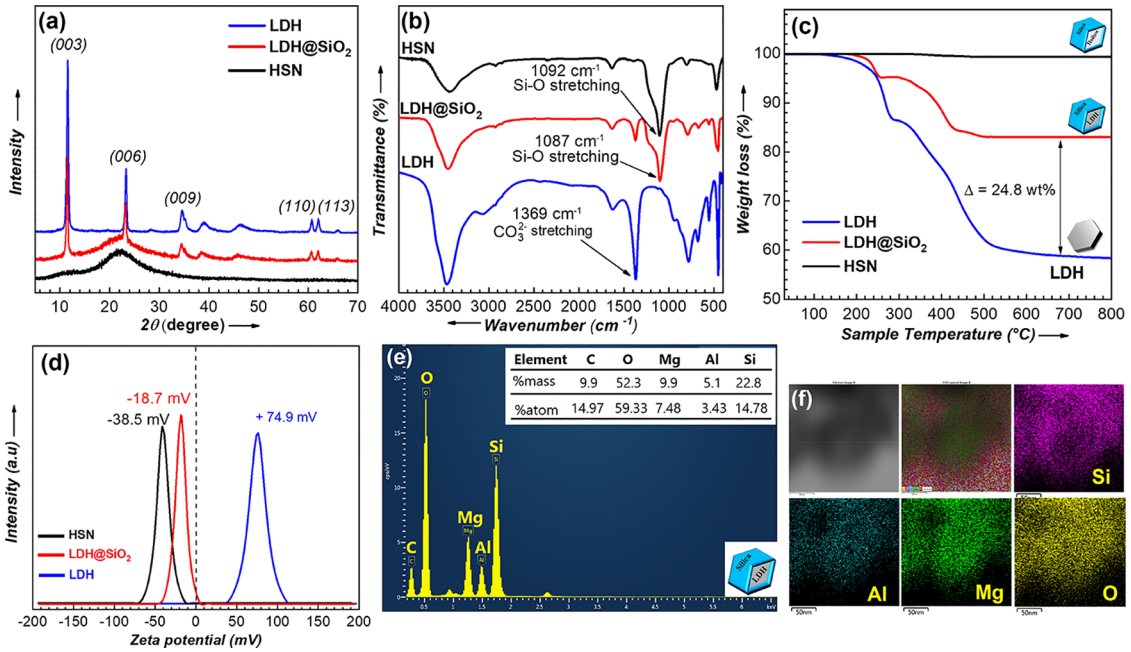

Figure 2. (a) XRD pattern, (b) FTIR spectrum, (c) TGA curve, (d) zeta potential of LDH, LDH@SiO_2 and HSN, (e) EDS spectrum, and (f) STEM and elemental mapping image for Si, O, Al, and Mg (f) of LDH@SiO_2.

the shell strength and reduces the properties of the materials in specific areas.[2,18−20] Furthermore, the release of CO_2 and waste organic solvent as byproducts during the removal of the polymer template is harmful to the natural environment in large-scale production.[17]

To address these challenges, researchers have focused on developing surfactant-free methods for preparing hollow particles from inorganic templates that meet criteria such as environmental friendliness and ease of implementation.[16,28] Recently, numerous reports have explored various types of templates, with an emphasis on their applicability. Some suggested templates include calcium carbonate,[16,29] ZnO,[30,31] and the sodium salt template.[32] In most studies, TEOS molecules are hydrolyzed to generate orthosilicic acid ($Si(OH)_4$), which condensed to form Si−O−Si bonds on the surface of templates to create core−shell particles.[33] Then, the template was removed by etching in aqueous HCl to obtain hollow particles. These approaches required an excessive amount of organic solvents such as ethanol and harmful chemicals such as hydrazine or ammonia to control the hydrolysis of TEOS, which increased the total cost of mass production.[23,33] Despite numerous investigations on the fabrication and use of hollow silica having been published, the production of HSN without the use of organic solvents remains limited.

In this study, we propose a surfactant-free method for the controllable synthesis of HSN using layered double hydroxide (LDH) nanoparticles as a hard template and sodium silicate (Na_2SiO_3) as the silica source. This investigation is the first to our knowledge to describe the formation of a SiO_2-coated LDH (LDH@SiO_2) core−shell structure by deposition of a silicate anion onto LDH templates, followed by acid treatment to obtain HSN. It can be more environmentally friendly than other traditional templates. In detail, this approach presents some advantages: (i) reducing the environmental impact compared to the traditional method by using LDH and Na_2SiO_3 precursors without any organic chemicals instead of PS and TEOS;[23] (ii) no surfactant is required to modify the template surface before coating with silicate anion due to the presence of a positive charge on LDH surfaces, resulting in the formation of hollow structures without mesopores; (iii) the size and shape of empty SiO_2 particles can be modified using various LDH templates, which can be further tailored by adjusting the hydrothermal temperature; (iv) the LDH templates can be easily removed by etching in aqueous HCl, and the etchant solution can be reused for the synthesis

https://doi.org/10.1021/acsomega.3c03917
ACS Omega 2023, 8, 31399−31409

template; (v) the shell thickness of HSN can be manipulated by adjusting the silicate concentration. All of these factors make this approach a good candidate for large-scale production of HSNs, where cutting costs is a top priority. The resultant HSN has low thermal conductivity and high light reflection properties. The simulation test was also used to investigate the effect of HSN on the features of epoxy/HSN composites. The outcomes demonstrated that HSNs are an effective filler for thermal insulation coatings.

2. RESULTS AND DISCUSSION

2.1. Characterization and Formation Mechanisms of HSN. A strategic multistep method was used to design and prepare the HSN, as illustrated in Figure 1. The carbonated-MgAl LDHs were synthesized using the coprecipitation approach, wherein the shape and particle size of LDH are manipulated by adjusting the aging temperature. The LDH coating was conducted with Na_2SiO_3 at pH 9−10, and then, the core was removed to obtain HSN by acid treatment. The characteristics of LDH, LDH@SiO_2, and HSN obtained from this process are illustrated in Figure 2. The XRD patterns of LDHs revealed well-defined diffraction peaks at 2θ: 11.81°, 23.55°, 34.74°, 60.91°, and 62.21°, which were assigned to (003), (006), (009), (110), and (113) planes (as shown in Figure 2a), respectively, and matched well with the MgAl−CO_3 LDH standard [JCPDS Card No. 51-1528].[34] In addition to the above, the basal spacing d(003) = 0.763 nm was determined by Bragg's law, indicating the MgAl−CO_3 LDH was successfully synthesized.[35] The high specific peak intensity and absence of impurity peaks indicate that it possessed good crystallinity and high purity of the LDH phase. In comparison, the XRD patterns of LDH and LDH@SiO_2 showed the position of diffraction peaks did not change significantly during the coating process. This indicates that there is no intercalation of any anion into the interlayer space of LDH and confirms that the LDH structure was preserved during the coating process.[30] Furthermore, with the coating of silicate surrounding the LDH core, the unidentified noise was detected at an angle below 30° of the core−shell sample, which could point out the formation of an amorphous structure.[33] After the etching stage, the LDH peaks disappeared, leaving a wide diffraction peak in the region of 2θ 10−30°; the observed phase was represented as an amorphous structure of SiO_2.[29] The Mg and Al cations released after the etching process could be easily separated from the suspension by a vacuum filter funnel. The collected cations were reused for the synthesized LDH template. The FE-SEM image of the recycling template revealed a well-defined morphology, and XRD analysis revealed that the diffraction angle peaks corresponded well to the MgAl−CO_3 LDH standard (Figure S1). These results confirmed the successful reuse of cations for the next synthesis template, which can be attributed to the cost-effectiveness of the process using LDH templates for synthesizing hollow particles.

The development of the SiO_2 layer on the surface of LDHs was additionally investigated by the FTIR spectrum (displayed in Figure 2b), which revealed significant changes in absorption peaks. In the LDH and LDH@SiO_2 samples, the strong absorption at 3454 cm^{-1} is related to the OH-groups that bind to metal ions present in the brucite-type layer. Additionally, a small oscillation role at a frequency of 2925 cm^{-1} is typical for the bending vibrations of the H-bond formed between water and the carbonate anion. The strong absorption peak at 1371 cm^{-1} is associated with the vibration mode of the carbonate group, while the peaks at 553 and 678 cm^{-1} are related to metal−oxygen stretching vibration in the octahedral layers of LDH.[36,37] In the case of coated particles, a significant absorption band was observed in the range 1300−700 cm^{-1}, pointing to the presence of silica. The LDH@SiO_2 absorption bands appeared at 1087 cm^{-1} in response to the Si−O−Si stretched vibrating,[38,39] confirming the successful coating of LDH nanoparticles with SiO_2. After the etching process, the hydroxyl group still existed on the surface of the hollow silica nanoparticle, as demonstrated by the band at 3411 cm^{-1}.[37] Antisymmetric stretching and bending vibration peaks of Si−O−Si remained to be 1092 cm^{-1}.[38,39] The disappearance of the carbonate absorption peaks at 1371 cm^{-1} indicates that the LDH template was eliminated by acid treatment. These FT-IR outcomes are in conformance with XRD analysis results.

The amount of silica coating on the surface of LDHs was determined by using TGA analysis (Figure 2c). During the increase of temperature to 800 °C, the weight loss of the LDH template was found to be approximately 42.5%, which is well matched with the previous report.[40] In the case of the LDHs@SiO_2 core−shell system, the weight loss was about 17.7%, and this assumes that 24.8 wt % of silica is presented in the product obtained from the coating process. The reduced weight of the product obtained from the etching treatment did not change significantly, this result indicating that the LDH cores are eliminated during the etching treatment.

The surface charge existing in the prepared particles was determined by zeta potential and is illustrated in Figure 2d. The template exhibited a high positive zeta potential (+74.9 mV), showing the stability of the suspension. Xu et al. found that during the hydrothermal treatment, the cation was distributed more evenly in hydroxide layers, promoting the development of isolated crystallizes through the diffusion of cations and crystallite refining.[41] As a result, the LDH nanoplates can remain stable and resist aggregation by Brownian motion, forming a stable colloid. Similar outcomes were reported recently, showing that the stable homogeneous suspensions of LDHs were maintained even after 90 days of storage, which supports the idea of using LDH nanoplates in large-scale applications.[42] After coating with silicate, the surface charge was measured to be negative (−18.7 mV), which is consistent with the dissociation of the silanol group (≡Si−OH) on the template surface.[33] This observation was further supported by the FTIR spectra. The zeta potential of the core−shell structure was found to be less negative than that of hollow particles (−38.9 mV). We propose that the removal of the heavy core results in lighter HSN, which reduces the tendency to aggregate in water. In addition, due to the high concentration of silicate precursor, more SiO_2 particles can be packed into the nanoshell, resulting in a higher nanoshell density. This density increased the value of negative charge due to a greater number of ≡SiO^- groups available on the surface of particles,[43] given the increasing of zeta potential to a more negative value (Table S1). However, it should be noted that when the concentration of Na_2SiO_3 exceeded 1.0 M, the negative zeta potential decreased. This implies that the onset of agglomeration may be occurring in this sample.

The analysis results provided evidence that the LDH template, LDH@SiO_2, and HSN were successfully prepared. The fabrication mechanism of silica on the LDH template can be explained as follows. The dropwise introduction of an initial silicate solution into an aqueous synthesis medium increased

https://doi.org/10.1021/acsomega.3c03917
ACS Omega 2023, 8, 31399−31409

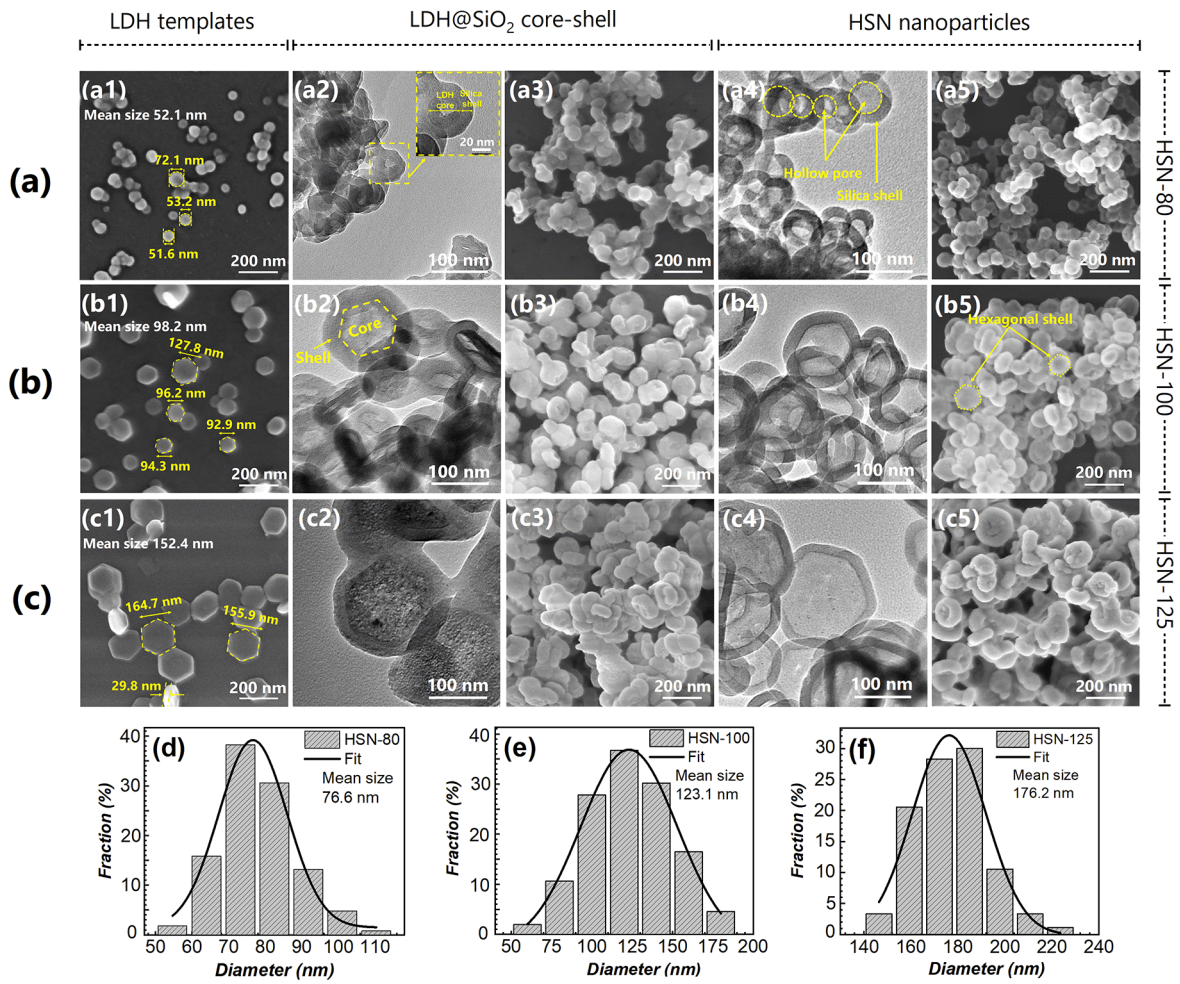

Figure 3. FE-SEM images of LDHs (a1−c1), LDHs@SiO_2 (a3−c3), HSNs (a5−c5), and TEM images of LDH@SiO_2 (a2−c2), HSNs (a4−c4); the size distribution of HSN-80 (d), HSN-100 (e), and HSN-125 (f). Series pictures a, b, and c denoted for the prepared samples using LDH-80, LDH-100, and LDH-125 templates, respectively.

the dissociation level of Na_2SiO_3, resulting in the formation of a large amount of silicate anion (≡Si−O^-), which was deposited directly on the positive charge surface of LDH via electrostatic interactions. Simultaneously, the silicate anion is hydrolyzed into a silica monomer as silicic acid (≡Si−OH), as in eq 1. It should be emphasized that the isoelectric point of silica appears in acidic regions, so maintaining pH at weakly basic conditions leads to the partially deprotonated silanol group. The coexistence of large quantities of silicic acid monomers and silanol anion facilitated the fast condensation reaction to produce siloxane bonds (≡Si−O−Si ≡), resulting in the formation of silica networks surrounding the LDH core, as shown in eq 2.

$$\equiv Si - O^- + H_2O \rightarrow \equiv Si - OH + OH^- \quad (1)$$

$$\equiv Si - OH + {}^-O{-}Si\equiv \rightarrow \equiv Si - O - Si\equiv + OH^- \quad (2)$$

Subsequently, prepared LDH@SiO_2 was treated with HCl, in which the template was etched by acid dissolution, resulting in the formation of porous silica particles.

In addition, the structure and element composition of the core−shell system were further clarified by the EDS and STEM mapping, which are presented in Figure 2e,f, respectively. Mg and Al elements are mainly distributed in the central region of LDH@SiO_2, while Si and O cover all of the particles, especially in the periphery of the particle. This confirmed that a core−shell structure was formed following the coating process. EDS results confirmed the highly purified composition of the core−shell particle. The molar ratio of Mg/Al is 2.18, close to the theoretical ratio used for synthesizing LDH, and it should be emphasized that the components do not contain the Cl- anion. Iyi et al. demonstrated that the decarbonation of the LDHs does not occur when exposed to an alkaline medium.[44,45] This explained that there was no interlacing of the anion into the basal spacing of LDH during the modification process, which was verified by XRD analysis.

2.2. Morphology and Size Control of HSN. The study also investigated the deposition of silica on templates with varying sizes and morphologies. Figure 3 illustrates the electron microscopy image of the synthesized particles. The FE-SEM image of the template, as depicted in Figure 3a1−c1, revealed the size and shape of LDH depending on the aging temperature. At a temperature of around 80 °C, the LDH templates presented a spherical shape with a mean size centered at around 52.1 nm. As the temperature increased, a well-defined hexagonal shape emerged with a particle size that also rose to 98.2 and 152.4 nm, corresponding to hydrothermal temperatures of 100 and 125 °C, respectively. In all cases, a homogeneous distribution was observed, indicating that the traditional nucleation followed by aging treatment under

https://doi.org/10.1021/acsomega.3c03917
ACS Omega 2023, 8, 31399−31409

continuous stirring can produce uniform particles of MgAl-LDH at high concentrations, which are suitable for mass production of LDH.

Upon coating with Na_2SiO_3, the obtained samples retained the morphology of the LDH templates and exhibited a typical core−shell structure, which was confirmed by TEM observations, as shown in Figure 3a2−c2. A distinct contrast line was observed, implying complete coverage between the core and shell and demonstrating a well-distributed coating layer on the template surface. The FE-SEM image, as displayed in Figure 3a3−c3, revealed a rough surface of the silica shell, which can be ascribed to the etching effect induced by the injection of acid during the Na_2SiO_3 titration process.[33] This phenomenon was observed across all types of templates. In addition, the low-magnification FE-SEM image (Figure S2) revealed that the silica coating is homogeneous, suggesting that the silicate anion can be deposited uniformly on the LDH surfaces without the use of a surfactant.

After the acid treatment, the morphology of the resultant HSN nanoparticles was distinguishable on TEM due to the contrast between the light core and dark edge, as illustrated in Figure 3a4−c4. This contrast pointed out the removal of LDH cores. It should be noted that the hollow cavities matched the shape of the templates. Additionally, The TEM analysis unveiled the integrity of the silica shells in HCl aqueous solution, as evidenced by the entirety of the shell curve. FE-SEM images further supported this observation, as shown in Figure 3a5−c5. The resultant HSNs exhibited a uniform distribution, with particle sizes of approximately 76.6, 123.1, and 176.2 nm, corresponding to the three types of LDH employed in the synthesis.

Nitrogen adsorption was utilized to analyze the specific surface area (S_{BET}) of LDH and HSN. The S_{BET} values for LDH-80, LDH-100, and LDH-125 were determined to be 84.81, 71.34, and 70.18 m^2/g, respectively. These measurements indicated that surface area decreased when the particle size increased. Following the etching process, the S_{BET} of resulting hollow particles increased to 128.9, 122.4, and 116.3 m^2/g, corresponding to mean particle sizes of HSN at about 76.6, 123.1, and 176.2 nm, respectively. The nitrogen absorption isotherm of HSN-125 (Figure 4a) is classified as type II according to the IUPAC classification, which is consistent with previous reports on mesopore-free material.[18,19,46] Figure 4b displays the pore size distribution of the hollow particle measured by the BJH method. The resultant HSN-125 exhibited a broad distribution of pore sizes centered at around 167.5 nm, aligning well with the hollow core observed through TEM. This phenomenon was also found in the cases of HSN-80 and HSN-100 (Figure S3). Furthermore, no identified peaks were observed that could represent the mesopore channel in the silica shell, providing further confirmation of the mesopore-free structure of the hollow particles prepared for this investigation.

2.3. The Effect of Shell Thickness on the Light Reflectance of HSN. For investigating the effect of Na_2SiO_3 concentration on the shell thickness (T_s) and the light reflectance effect of HSN nanoparticles, a series of experiments were conducted using the LDH-125 template with various concentrations of the silicate precursor. The shell thickness was determined by analyzing TEM images, where a black-shaded ring was used to enclose the hollow core and measure the shell thickness of the nanoparticles, as illustrated in Figure 5a−e. As the concentration of Na_2SiO_3 increased

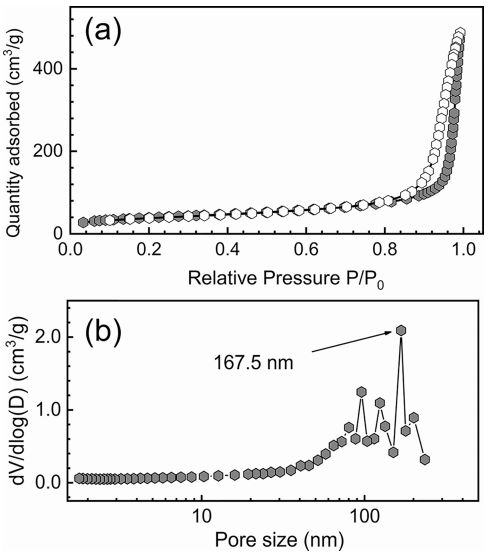

Figure 4. Nitrogen adsorption−desorption isotherm curve (a) and pore size distribution (b) of HSN-125.

from 0.5 to 0.75 1.0, 1.25, and 1.5 M, the T_s value also increased from 6.8 to 12.1 17.1, 20.8, and 22.5 nm, respectively. Even though the thickness of the shell of HSN can be modified by varying the amount of silica precursor, those are not linear with each other. At concentrations higher than 1.0 M, the increase in T_s exhibited a slower trend compared with lower concentrations. This observation can be attributed to the fact that at higher concentrations of silica precursors, certain SiO_2 monomers nucleate in the aqueous medium instead of depositing on the LDH surface.[31] As a result, the growth of the silica shell thickness becomes limited.

UV−vis−NIR spectroscopy was utilized for evaluating the positive aspect of a hollow structure compared to a solid one for reflected solar light as well as the influence of the particle size and shell thickness on solar reflectance (Figure 6a−c). The silica density of Konasil K-200, with an average size of the particle of 40 nm, was also analyzed for comparison, and the summarized results of the HSN series are also listed in Table 1. All of the samples exhibited a noticeably lower reflectance in the near-infrared light range while maintaining greater reflectance in the UV−visible region, which corresponds with the characteristic of hollow silica, as shown in the previously reported studies.[21]

According to the Mie scattering theory, light scattering is greatly influenced by the size and shape of the nanoparticles. The scattering efficiency occurs when the particle sizes are roughly comparable to the wavelength (λ) of the incident light.[22,43] This phenomenon explained the increased intensity of reflectance spectra corresponding with a larger size of HSN. Analysis results revealed that the average total light reflectance (ALR) values of HSN-80, HSN-100, and HSN-125 are 66.63, 68.50, and 73.45%, respectively. In comparison, solid silica, which possesses a higher density and refractive index, exhibits an ALR value of only 46.63%. This significant difference is a result of the distinctive structure of HSN, which consists of a hollow interior with a low refractive index and a silica shell with a high refractive index. The interface between these two phases provides efficient sites for enhancing light scattering efficiency, resulting in increased light reflectance.[17,47] In addition, the effect of shell thickness on the reflective property

https://doi.org/10.1021/acsomega.3c03917
ACS Omega 2023, 8, 31399−31409

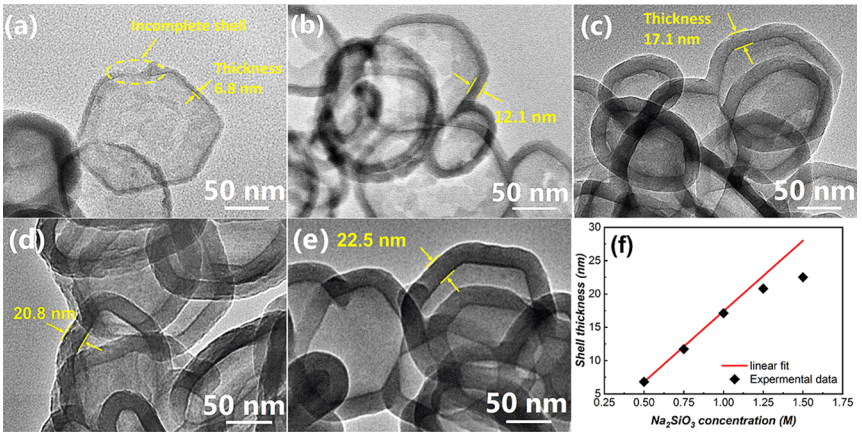

Figure 5. TEM images of HSN-125 were synthesized by using various concentrations of Na_2SiO_3: 0.5 (a), 0.75 (b), 1.0 (c), 1.25 (d), and 1.5 M (e), and the correlation between Na_2SiO_3 concentration and the shell thickness of hollow particles, as measured from TEM observations (f).

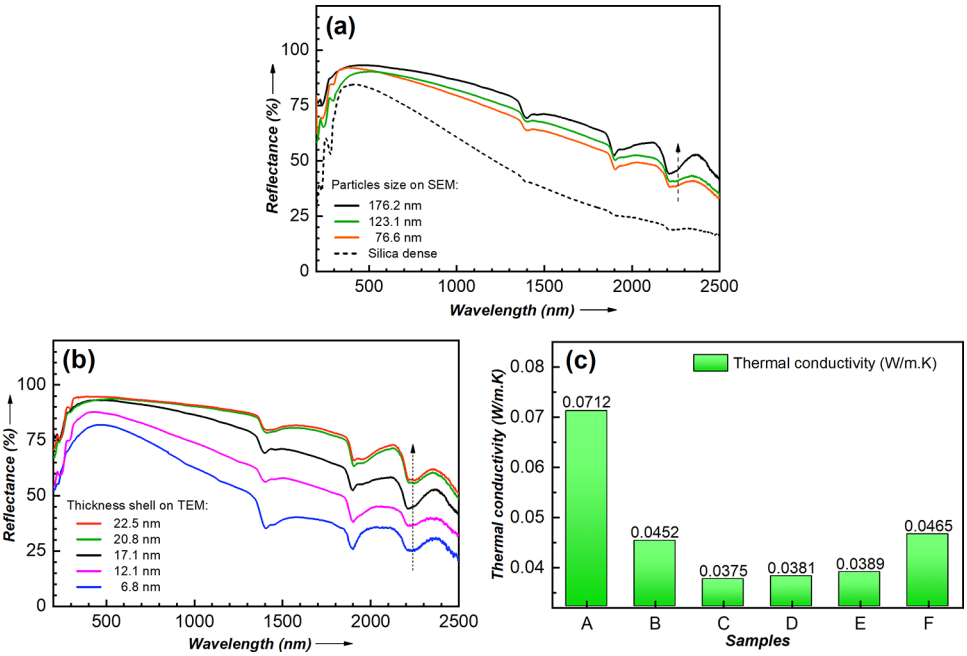

Figure 6. Reflectance spectrum of HSN nanoparticles with various particle sizes, in comparison with silica dense (a); HSN-125 with different shell thicknesses (b); the thermal conductivity of prepared particles included LDH-125 (A), LDH@SiO_2-125 (B), HSN-80 (C), HSN-100 (D), HSN-125 (E) and silica dense (F).

Table 1. Light Reflectance Values of HSNs Synthesized at Various Size and Shell Thickness

samples	core morphology	core size (nm)	shell thickness (nm)	average of light reflectance (%)
silica dense ($d \sim 40$ nm)	-	-	-	46.63
HSN-80	spherical	52.1	15.1	66.63
HSN-100	hexagonal	98.2	19.8	68.50
HSN-125	hexagonal	152.4	17.1	73.45
HSN-125	hexagonal	152.4	6.8	51.07
HSN-125	hexagonal	152.4	12.1	61.77
HSN-125	hexagonal	152.4	20.8	79.98
HSN-125	hexagonal	152.4	22.5	82.10

of HSN was also investigated and is displayed in Figure 6b. The result revealed that there is a direct correlation between shell thickness and solar reflectance. HSN with thicker shells exhibited higher solar reflectance. The ALR values of HSN with shell thicknesses of approximately 6.8, 12.1, 17.1, 20.8, and 22.5 nm were measured as 51.07, 61.77, 73.45, 79.98, and 82.10%, respectively. The increasing trend indicates that the reflectance property can be assigned to the amount of SiO_2 coverage on the nanoparticle surface.[43,48] It is assumed that as the density of the SiO_2 shell increases, a greater difference in the refractive index between the core and shell occurs, thereby leading to an increase in the reflectance value. Taken together, these findings further suggested the advantages of HSN with thicker shells, which offer enhanced mechanical stability, making them preferable for various applications compared with those with thinner shells.

Thermal conductivity is a crucial factor in determining the efficiency of hollow particles. Initially, the LDH core exhibited a thermal conductivity of approximately 0.0712 W/m·K, which decreased to 0.0452 W/m·K after coating with a silicate solution. The removal of the solid core resulted in a further

https://doi.org/10.1021/acsomega.3c03917
ACS Omega 2023, 8, 31399−31409

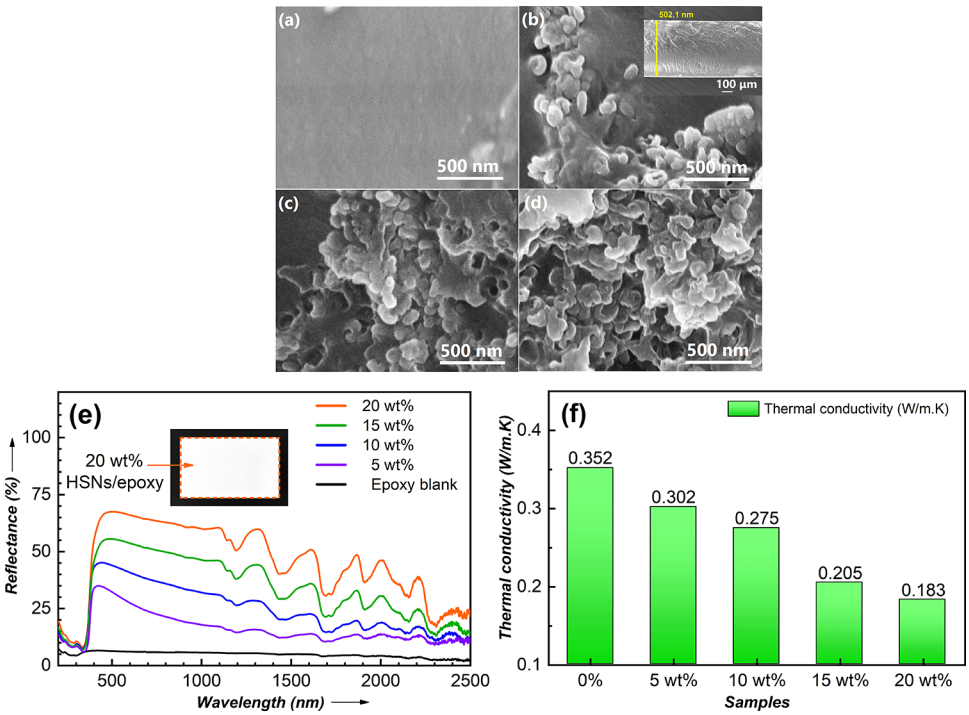

Figure 7. FE-SEM image of epoxy membranes with different amounts of HSN: 0 wt % (a), 5 wt % (b), 10 wt % (c) and 20 wt % (d); light reflectance spectrum (e) thermal conductivity of epoxy membranes with various HSN amounts (f).

decrease in thermal conductivity. In this study, the difference in thermal conductivity among the HSNs was not significant, varying from 0.0375 to 0.0389 W/m·K (as shown in Figure 6c). This represents a notable improvement compared to the hollow silica with a consistent mesoporous structure at the same particle size and shell thickness, as reported in the literature.[26] In comparison to HSNs with larger diameters, HSN-80 exhibited a lower thermal conductivity. This phenomenon is consistent with the Knudsen effect, which occurs when the pore size is lower than twice the average free path of air (i.e., 134 nm). In such cases, the thermal motion of air molecules is effectively restricted, reducing the probability of collisions between molecules and consequently reducing heat transfer.[17] For comparison, the thermal conductivity of solid nano silica is approximately 0.0465 W/m·K, which is roughly 20% greater than that of the hollow structure. This finding confirmed the significant impact of the hollow structure on the interruption of heat transfer within the HSN, demonstrating its potential as an effective thermal insulation filler.

These results demonstrated that not only the hollow cavity but also the solid shell of the HSN is effective at enhancing the thermal insulation effect. This improvement can be attributed to two key working mechanisms: (1) as a reflective filler, when the light source hits the coating surface, the shell layer will reflect and scatter the light, thereby slowing down the accumulation of heat and contributing to the reduction of heat adsorption by the materials; (2) as a barrier filler, the hollow interior stores a lot of air which reduces the thermal diffusion between solids due to the presence of gas pores in the insulation films.[17,21] This suggested that hollow silica is an ideal candidate for the preparation of insulation coatings.

2.4. Preparation of Epoxy/HSN Insulation Films. HSN 125 was selected for application in thermal insulation films due to its highest ALR value and no significant difference in thermal conductivity compared with other HSN samples. During incorporation into the epoxy matrix, porous particles with low shell thickness can be broken under mechanical stress, and broken particles considerably impact the thermal conductivity of composites.[49] To address this issue, we used hollow particles such as HSN-125 with the highest shell thickness (22.5 nm) to prepare the composite films. The epoxy suspension was prepared by stirring with a magnetic stirrer for 1 day before adding the hardener to obtain a more even distribution of the silica. Then, the mixture was applied to an aluminum plate to initiate the curing reaction. It should be emphasized, due to the low density of HSN, that the HSN:epoxy volume ratio rises significantly with increasing HSN quantity. This substantially increases the epoxy/HSN suspension viscosity, making it challenging to obtain a well-dispersed HSN in the epoxy matrix before curing. Therefore, the maximum content of HSN was limited to 20 wt %; higher levels led to films being more prone to cracking during the curing process.

The surface morphology (at cross section) of insulation films is observed by FE-SEM and the images are displayed in Figure 7a–d. As shown in Figure 7a, in the absence of hollow particles, the surface of the neat epoxy was clear and smooth. Compared to the SEM image of insulation films in Figure 7b–d, it can be observed that the packing density of nanoparticles increases considerably during the rising mass proportion of HSNs. Furthermore, only a few broken particles were observed, which confirmed the stability of the thick shell structure under vigorous mechanical stirring. It should be noted that the dispersibility of the filler is a critical factor in influencing the characteristics of the coating films.[12,31] To study the distribution level of HSN filler in the epoxy matrix, the EDS mapping analysis was performed on the sample containing 10 wt % HSN. The result revealed that the HSNs

https://doi.org/10.1021/acsomega.3c03917
ACS Omega 2023, 8, 31399−31409

were dispersed evenly in the epoxy matrix, forming a relatively dense film (Figure S4).

The light reflectance spectra of the epoxy films with various contents of HSN are illustrated in Figure 7e, and ALR values are listed in Table 2. The results showed that the addition of

Table 2. Average of Total Light Reflectance and Thermal Conductivity of Epoxy/HSN Films

Sample	ALR value (%)	Thermal conductivity (W/m.K)
blank epoxy	4.87	0.352
5 wt % of HSN	16.10	0.302
10 wt % of HSN	24.29	0.275
15 wt % of HSN	33.95	0.205
20 wt % of HSN	45.26	0.183

HSN improved the light reflectance properties of the epoxy composite films. In comparison, the blank epoxy film only achieved a light reflectance of 4.87%, while the composite films showed higher ALR values and reached the highest at 45.26%, corresponding with 20 wt % of HSN. The thermal conductivities of epoxy/HSN composites were also displayed in Figure 7f. The results revealed that, after the introduction of HSN, the thermal conductivity of the epoxy film was significantly reduced by about 50%, from 0.352 to 0.183 W/m K. This might be explained by the increasing porous space in the coating layer and further confirmed the positive effect of HSN on the thermal insulation property of composite films.

To investigate the heat transfer capacity of epoxy/HSN insulation coatings, a series of experiments were conducted to measure the surface temperature of coatings exposed to infrared lamp radiation. The results presented in Figure 8,

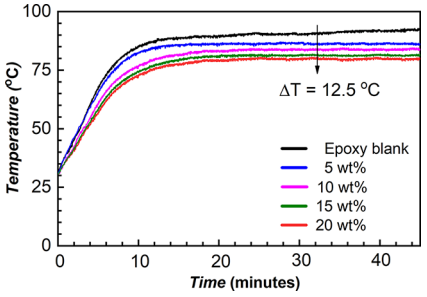

Figure 8. Surface temperature of epoxy films containing different amounts of HSNs under infrared lamp radiation.

reveal interesting findings. Initially, it was observed that the surface temperature of neat epoxy coating gradually increased after 15 min of radiation and remained higher compared to samples containing HSN. As the content of HSN increased, the surface temperature of the coatings decreased. In particular, the coating containing 20 wt % of HSN exhibited the lowest surface temperature at about 77.6 °C, cooler than the neat epoxy coating at about 12.5 °C. This temperature reduction can be attributed to the low thermal conductivity of the insulation film. Furthermore, the coating displays a high level of whiteness, indicating heat reflection properties, which aligns with the results shown in Figure 7e, where 20 wt % HSN coating demonstrated the highest reflectivity. The findings collectively provide compelling evidence of the potential of hollow silica particles produced from LDH templates as insulation additives for applications where low heat transfer is desired.

3. CONCLUSIONS

In conclusion, hollow silica nanoparticles with a controllable particle diameter and shell thickness were successfully synthesized through a surfactant-free synthesis approach utilizing layered double hydroxide templates. The silica shell was deposited without the use of a surfactant due to the high positive charge on the surface of LDHs. We achieved precise control over the particle diameters ranging from 50 to 200 nm by manipulating the size of the template. In addition, by adjusting the concentration of Na_2SiO_3, the shell thickness of the HSNs was tunable within a range of 6.8−22.5 nm. The integrity of the silica shell without the mesopore channel was preserved during the etching process by adding aqueous HCl slowly. The combination of a hollow interior and a solid silica shell in the HSN contributed to their low thermal conductivity and high light reflection properties. In simulation tests, the epoxy/HSN composite exhibited superior thermal insulation capabilities, resulting in a surface temperature decrease of approximately 12.5 °C compared with a blank epoxy. This study demonstrates the potential of the cost-effective method for synthesizing HSN, making them promising candidates for thermal insulation materials.

4. EXPERIMENTAL SECTION

4.1. Materials. Aluminum chloride hexahydrate ($AlCl_3.6H_2O$, 99%), and magnesium chloride hexahydrate ($MgCl_2·6H_2O$, 98%) were obtained from Alfa Aesar. Sodium hydroxide (NaOH, 98%), sodium carbonate (Na_2CO_3, 99.5%), hydrochloric acid (HCl 36.5%), and lactic acid ($C_3H_6O_3$, 88%) were purchased from Scharlau. A commercial grade of Na_2SiO_3 (sodium silicate solution Na_2O 9−10%, SiO_2 26−28%) was obtained from Vinachem.

The insulation film base on the epoxy system, which included epoxy bisphenol A (D.E.R-331) and polyamine hardener (XUS 19036.00) were purchased from Dow Chemical. Industrial-grade of solvent used for dilution as methyl isobutyl ketone (MIBK) was purchased from Kumho P&B Chemicals (Korea). All the chemicals were used as received.

4.2. Preparation of LDH Templates. Three primary processes were required to prepare the hollow silica particles, including LDH preparation, silica coating, and etching template. The coprecipitation technique was used to create the LDH templates, as described in our previous report.[42] In order to prevent CO_2 from entering suspension during the coprecipitation, lactate anion was added. In detail, 150 mL of 2.4 M NaOH solution was added to 200 mL of salt solution containing 0.5 M $MgCl_2$, 0.25 M $AlCl_3$, and 0.5 M sodium lactate (equivalent by NaOH from lactic acid) while stirring vigorously to achieve pH 10. The precipitate was exchanged in 500 mL of 0.15 M Na_2CO_3 for 30 min. Then, the carbonate-loaded LDHs were isolated and redispersed in DI water by homogenization at 16,000 rpm for 15 min to yield a 5 wt % of LDHs in suspension. The obtained suspension was aged for 24 h with stirring at 250 rpm in a high-pressure reactor (4520 Bench Top reactor, Parr Instrument) at a defined temperature. Following hydrothermal treatment, the LDH products were washed and redispersed in DI water to obtain 5 wt % of LDHs, which was used as the template for the preparation of hollow silica. To regulate the particle size of the template, the aging temperature was varied between 80, 100, and 125 °C.

https://doi.org/10.1021/acsomega.3c03917
ACS Omega 2023, 8, 31399−31409

4.3. HSNs Synthesis. The SiO_2-coated LDH (LDH@SiO_2) core−shell particles were prepared by using a wet chemical deposition technique. A 250 mL LDH suspension was heated to 80 °C and adjusted to pH 9−10 with the addition of 1.0 M HCl. Then, 40 mL of 1.0 M Na_2SiO_3 was added dropwise into LDH suspension for 2 h. The 1.0 M HCl was added simultaneously to titration and kept the pH at the desired value. After titration time, the suspension was continuously aged for 2 h. The resultant core−shell particles were washed to neutral pH and redispersed in deionized water for subsequent uses. To tailor the shell-thickness of HSN, the concentration of Na_2SiO_3 solution was varied incrementally, ranging from 0.5 to 0.75, 1.0, 1.25, and 1.5 M.

To eliminate the LDH core, LDH@SiO_2 suspension was introduced with 2.0 M HCl solution at 80 °C to reach pH 1.0. The reaction was maintained for 8 h under stirring at 250 rpm and the obtained product was separated by a centrifuge to collect the hollow particles, which were washed with DI water to neutral pH before vacuum drying overnight at 80 °C.

The samples were designated as "sample type-T", where the sample type is LDH, LDH@SiO_2, or HSN, and T was the aging temperature of the LDH, which was used to prepare hollow particles (i.e., HSN-80).

4.4. Preparation of Epoxy/HSN Films. The epoxy/HSNs insulation films were prepared based on the incorporation of HSN with epoxy bisphenol A and polyamine hardener. In detail, MIBK was used to dilute D.E.R 331, resulting in a solution containing 62.5 wt % of epoxy (part A). Simultaneously, a curing solution with 7.5 wt % of hardener (part B) was produced by diluting the polyamine XUS 19036.00 in MIBK. The hollow silica was added to part A and dispersion overnight by vigorous magnetic stirring. Then, the curing solution was introduced in a weight ratio of 1:4. The epoxy/HSN suspensions were applied onto the aluminum sheets (150 mm × 100 mm × 0.8 mm) to form insulation films, which were cured at 60 °C in an oven. The obtained insulation films with a thickness of about 500 μm were stored for 7 days in air to ensure full curing before another measurement.

4.5. Analytical Characterizations. The crystal structures of the prepared nanoparticles were identified using X-ray powder diffraction patterns on the D8 Advance instrument, Bruker (Germany) with CuKa radiation (k = 1.5418 Å) in the range 2θ 5−70°. Fourier transform infrared (FT-IR) was analyzed in the range of 400−4000 cm^{-1} using an FT-IR spectrophotometer on Tensor 27, Bruker (Germany). Thermal gravimetric analysis method (TGA) on a LabSys Evo TG-DSC 1600 Setaram equipment (France) in temperatures of 30−800 °C at a heat rate of 10 °C/min in N_2. The surface charge of prepared nanoparticles was evaluated by using the zeta potential measurement on the SZ-100, Horiba (Japan), at 25 °C. The morphology, particle size, and shell thickness of the samples were observed by a field emission scanning electron microscope (FE-SEM) on a Hitachi SU 8010 (Japan) and transmission electron microscopy (TEM) on a JEOL JEM-2100 (Japan). The specific surface area, pore volume, and pore size distribution of the samples were collected from the N_2 isothermal adsorption experiment by BET and BJH analysis on a Tristar II Plus, Micrometrics (USA). Reflectance measurements were performed using UV−vis−NIR spectroscopy on Jasco V-770 (Japan) equipment in the range of 200−2500 nm, with $BaSO_4$ white plate used as reference. The average of total reflectance (200−2500 nm) was determined by dividing the sum of reflectance values by the number of wavelengths.[21]

The thermal conductivity of the powders and epoxy film samples was determined by a C-Therm Trident with an MTPS sensor (C-therm Technologies, Canada) at room temperature. The self-designed setup was developed to simulate the practical applications of epoxy/HSN films (as seen in Figure 9). This setup consists of a heat box (250 mm × 200 mm × 200 mm) insulated with polystyrene (25 mm thickness) and accompanied by a 200 W OSRAM infrared lamp. The test plates were positioned on top of the heat box, and a thermometer was placed in direct contact with the bottom of the aluminum plate coated with epoxy to monitor any temperature changes on the outer surface. The data were recorded continuously during 45 min of the test with 1 s of step time. Three replicates were performed on each test to ensure the reproductive.

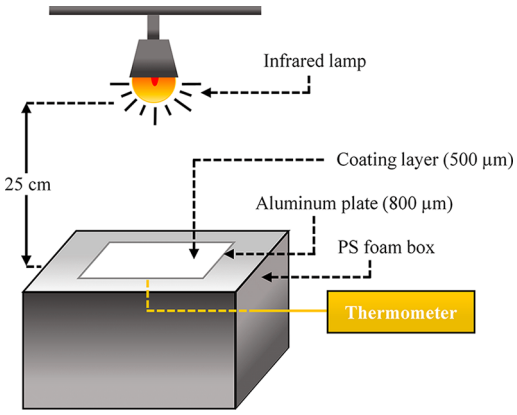

Figure 9. Self-setup device for simulating the thermal insulation effect of epoxy/HSN films.

■ ASSOCIATED CONTENT

Supporting Information

The Supporting Information is available free of charge at https://pubs.acs.org/doi/10.1021/acsomega.3c03917.

FE-SEM image and XRD pattern of recycling LDH template, low-magnified FE-SEM image of LDH@SiO_2-100, pore size distributions of HSN-80 and HSN-100 calculated from BJH analysis, EDS elemental mapping of the 10 wt % HSN/epoxy film, and the zeta potentials of prepared particles at various particle sizes and different coating conditions (PDF)

■ AUTHOR INFORMATION

Corresponding Author

Minh Vuong Phan − *Institute of Chemical Technology, Vietnam Academy of Science and Technology, Ho Chi Minh City 700000, Vietnam; Graduate University of Science and Technology, Vietnam Academy of Science and Technology, Hanoi 100000, Vietnam;* orcid.org/0009-0007-6431-1720; Email: pmvuong@ict.vast.vn

Authors

Thi Kim Thoa Tran − *Institute of Chemical Technology, Vietnam Academy of Science and Technology, Ho Chi Minh City 700000, Vietnam; Graduate University of Science and*

https://doi.org/10.1021/acsomega.3c03917
ACS Omega 2023, 8, 31399−31409

Technology, Vietnam Academy of Science and Technology, Hanoi 100000, Vietnam

Quynh Nhu Pham − *Institute of Chemical Technology, Vietnam Academy of Science and Technology, Ho Chi Minh City 700000, Vietnam*

Manh Huy Do − *Institute of Chemical Technology, Vietnam Academy of Science and Technology, Ho Chi Minh City 700000, Vietnam*

Thi Hong No Nguyen − *Institute of Chemical Technology, Vietnam Academy of Science and Technology, Ho Chi Minh City 700000, Vietnam; Graduate University of Science and Technology, Vietnam Academy of Science and Technology, Hanoi 100000, Vietnam*

Minh Ty Nguyen − *Institute of Chemical Technology, Vietnam Academy of Science and Technology, Ho Chi Minh City 700000, Vietnam*

Thanh Thao Phan − *Institute of Chemical Technology, Vietnam Academy of Science and Technology, Ho Chi Minh City 700000, Vietnam; Graduate University of Science and Technology, Vietnam Academy of Science and Technology, Hanoi 100000, Vietnam*

Thi Xuan Hang To − *Institute for Tropical Technology, Vietnam Academy of Science and Technology, Hanoi 100000, Vietnam; Graduate University of Science and Technology, Vietnam Academy of Science and Technology, Hanoi 100000, Vietnam*

Complete contact information is available at: https://pubs.acs.org/10.1021/acsomega.3c03917

Author Contributions

The manuscript was written through contributions of all authors.

Notes

The authors declare no competing financial interest.

■ ACKNOWLEDGMENTS

This research is funded by the Vietnam Academy of Science and Technology under grant number ĐLTE00.05/21-22. The authors would like to thank Dr. Thi Xuan Hang To and Dr. Thanh Thao Phan for their scientific support and the Institute of Chemical Technology for their support facilities.

■ REFERENCES

(1) Fuji, M.; Takai, C.; Tarutani, Y.; Takei, T.; Takahashi, M. Surface properties of nanosize hollow silica particles on the molecular level. *Adv. Powder Technol.* **2007**, *18* (1), 81−91.

(2) Bao, Y.; Shi, C.; Wang, T.; Li, X.; Ma, J. Recent progress in hollow silica: Template synthesis, morphologies and applications. *Microporous Mesoporous Mater.* **2016**, *227*, 121−136.

(3) Jiang, W.; Xiao, J.; Gao, X.; An, X.; Leng, Y.; Zhu, L.; Zhu, W.; Li, H. In situ fabrication of hollow silica confined defective molybdenum oxide for enhanced catalytic oxidative desulfurization of diesel fuels. *Fuel* **2021**, *305*, No. 121470.

(4) Florea, M.; Bocirnea, A.; Neaţu, S.; Kuncser, A. M.; Trandafir, M.-M.; Neaţu, F. Tuning the acidity by addition of transition metal to Mn modified hollow silica spheres and their catalytic activity in ethanol dehydration to ethylene. *Appl. Catal., A* **2022**, *646*, No. 118860.

(5) Shinde, P. S.; Suryawanshi, P. S.; Patil, K. K.; Belekar, V. M.; Sankpal, S. A.; Delekar, S. D.; Jadhav, S. A. A brief overview of recent progress in porous silica as catalyst supports. *J. Compos. Sci.* **2021**, *5* (3), 75.

(6) Shin, D.; Lee, S.; Jang, H. S.; Joo, J. B.; Choi, I. Redox/pH-dual responsive functional hollow silica nanoparticles for hyaluronic acid-guided drug delivery. *J. Ind. Eng. Chem.* **2022**, *108*, 72−80.

(7) Zou, Z.; Wen, S.; Li, Y.; An, J.; Wu, Q.; Tong, L.; Mei, X.; Tian, H.; Wu, C. Novel lactoferrin-functionalized manganese-doped silica hollow mesoporous nanoparticles loaded with resveratrol for the treatment of ischemic stroke. *Mater. Today. Adv.* **2022**, *15*, No. 100262.

(8) Kazemzadeh, P.; Sayadi, K.; Toolabi, A.; Sayadi, J.; Zeraati, M.; Chauhan, N. P. S.; Sargazi, G. Structure-property relationship for different mesoporous silica nanoparticles and its drug delivery applications: A review. *Front. Chem.* **2022**, *10*, No. 823785.

(9) Shah, I. U.; Jadhav, S. A.; Belekar, V. M.; Patil, P. S. Smart polymer grafted silica based drug delivery systems. *Polym. Adv. Technol.* **2023**, *34* (1), 24−43.

(10) Ali, A.; Saeed, S.; Hussain, R.; Afzal, G.; Siddique, A. B.; Parveen, G.; Hasan, M.; Caprioli, G. Synthesis and Characterization of Silica, Silver-Silica, and Zinc Oxide-Silica Nanoparticles for Evaluation of Blood Biochemistry, Oxidative Stress, and Hepatotoxicity in Albino Rats. *ACS. Omega.* **2023**, *8* (23), 20900−20911.

(11) Ernawati, L.; Ogi, T.; Balgis, R.; Okuyama, K.; Stucki, M.; Hess, S. C.; Stark, W. J. Hollow silica as an optically transparent and thermally insulating polymer additive. *Langmuir.* **2016**, *32* (1), 338−345.

(12) Xu, L.; He, J. Fabrication of highly transparent superhydrophobic coatings from hollow silica nanoparticles. *Langmuir.* **2012**, *28* (19), 7512−7518.

(13) Liu, H.; Tian, Y.; Mofid, S. A.; Li, S.; Zhou, J.; Hu, M.; Jelle, B. P.; Gao, T.; Wu, X.; Li, Z. Numerical modeling of effective thermal conductivity of hollow silica nanosphere packings. *Int. J. Heat. Mass. Transfer* **2022**, *182*, No. 122032.

(14) Sharma, J.; Polizos, G.; Jafta, C. J.; Bai, Y.; Hun, D.; Lyu, X. A lightweight thermally insulating and moisture-stable composite made of hollow silica particles. *RSC Adv.* **2022**, *12* (24), 15373−15377.

(15) Fuji, M.; Takai, C.; Watanabe, H.; Fujimoto, K. Improved transparent thermal insulation using nano-spaces. *Adv. Powder. Technol.* **2015**, *26* (3), 857−860.

(16) Nakashima, Y.; Takai, C.; Razavi-Khosroshahi, H.; Suthabanditpong, W.; Fuji, M. Synthesis of ultra-small hollow silica nanoparticles using the prepared amorphous calcium carbonate in one-pot process. *Adv. Powder. Technol.* **2018**, *29* (4), 904−908.

(17) Takai-Yamashita, C.; Fuji, M. Hollow silica nanoparticles: A tiny pore with big dreams. *Adv. Powder. Technol.* **2020**, *31* (2), 804−807.

(18) Nandiyanto, A. B. D.; Akane, Y.; Ogi, T.; Okuyama, K. Mesopore-free hollow silica particles with controllable diameter and shell thickness via additive-free synthesis. *Langmuir.* **2012**, *28* (23), 8616−8624.

(19) Nandiyanto, A. B. D.; Iwaki, T.; Ogi, T.; Okuyama, K. Mesopore-free silica shell with nanometer-scale thickness-controllable on cationic polystyrene core. *J. Colloid Interface Sci.* **2013**, *389* (1), 134−146.

(20) Kurimoto, M.; Kato, T.; Yoshida, T.; Kato, C.; Suzuoki, Y. Low permittivity epoxy nanoporous composites filled with hollow nanosilica. *IET Nanodielectr.* **2019**, *2* (3), 109−113.

(21) Bao, Y.; Guo, R.; Ma, J. Hierarchical flower-like hollow SiO_2@TiO_2 spheres with enhanced thermal insulation and ultraviolet resistance performances for building coating. *ACS Appl. Mater. Interfaces* **2020**, *12* (21), 24250−24261.

(22) Kim, J.; Lee, C.; Suh, Y. J.; Chang, H.; Roh, K.-M.; Jang, H. D. Synthesis and characterization of highly reflective hollow silica particles. *Mater. Res. Bull.* **2015**, *70*, 184−189.

(23) Gao, T.; Jelle, B. P.; Sandberg, L. I. C.; Gustavsen, A. Monodisperse hollow silica nanospheres for nano insulation materials: synthesis, characterization, and life cycle assessment. *ACS Appl. Mater. Interfaces* **2013**, *5* (3), 761−767.

(24) Sandberg, L. I. C.; Gao, T.; Jelle, B. P.; Gustavsen, A. Synthesis of hollow silica nanospheres by sacrificial polystyrene templates for

thermal insulation applications. *Adv. Mater. Sci. Eng.* **2013**, *2013*, No. 483651.
(25) Gao, T.; Sandberg, L. I. C.; Jelle, B. P. Nano insulation materials: Synthesis and life cycle assessment. *Procedia CIRP* **2014**, *15*, 490−495.
(26) Yang, Y.; Li, F.; Xiao, M.; Zhang, Z.; Wei, J.; Hu, J.; Yu, Q. TEOS and Na_2SiO_3 as silica sources: study of synthesis and characterization of hollow silica nanospheres as nano thermal insulation materials. *Appl. Nanosci.* **2020**, *10*, 1833−1844.
(27) Vu, K. B.; Phung, T. K.; Tran, T. T.; Mugemana, C.; Giang, H. N.; Nhi, T. L. P. Polystyrene nanoparticles prepared by nano-precipitation: A recyclable template for fabricating hollow silica. *J. Ind. Eng. Chem.* **2021**, *97*, 307−315.
(28) Wang, Y.; Su, X.; Ding, P.; Lu, S.; Yu, H. Shape-controlled synthesis of hollow silica colloids. *Langmuir.* **2013**, *29* (37), 11575−11581.
(29) Fuji, M.; Shin, T.; Watanabe, H.; Takei, T. Shape-controlled hollow silica nanoparticles synthesized by an inorganic particle template method. *Adv. Powder. Technol.* **2012**, *23* (5), 562−565.
(30) Qomariyah, L.; Arif, A. F.; Widiyastuti, W.; Winardi, S.; Taniguchi, S.; Ogi, T. Hexagonal hollow silica plate particles with high transmittance under ultraviolet-visible light. *RSC. Adv.* **2018**, *8* (46), 26277−26282.
(31) Cao, K. L. A.; Taniguchi, S.; Nguyen, T. T.; Arif, A. F.; Iskandar, F.; Ogi, T. Precisely tailored synthesis of hexagonal hollow silica plate particles and their polymer nanocomposite films with low refractive index. *J. Colloid Interface Sci.* **2020**, *571*, 378−386.
(32) Li, C.; Yao, J.; Huang, Y.; Xu, C.; Lou, D.; Wu, Z.; Sun, W.; Zhang, S.; Li, Y.; He, L. Salt-templated growth of monodisperse hollow nanostructures. *J. Mater. Chem. A* **2019**, *7* (4), 1404−1409.
(33) Cha, J. H.; Choi, H.-H.; Jung, Y.-G.; Choi, S.-C.; An, G. S. Novel synthesis of core−shell structured Fe_3O_4@SiO_2 nanoparticles via sodium silicate. *Ceram. Int.* **2020**, *46* (10), 14384−14390.
(34) Chen, B.; Sun, Q.; Wang, D.; Zeng, X. F.; Wang, J. X.; Chen, J. F. High-gravity-assisted synthesis of surfactant-free transparent dispersions of monodispersed MgAl-LDH nanoparticles. *Ind. Eng. Chem. Res.* **2020**, *59* (7), 2960−2967.
(35) Cavani, F.; Trifiro, F.; Vaccari, A. Hydrotalcite-type anionic clays: Preparation, properties and applications. *Catal. Today* **1991**, *11* (2), 173−301.
(36) Fajrina, N.; Yusof, N.; Ismail, A.; Jaafar, J.; Aziz, F.; Salleh, W.; Nordin, N. MgAl-CO_3 layered double hydroxide as potential filler in substrate layer of composite membrane for enhanced carbon dioxide separation. *J. Environ. Chem. Eng.* **2021**, *9* (5), No. 106164.
(37) Bernard, E.; Zucha, W. J.; Lothenbach, B.; Mäder, U. Stability of hydrotalcite (Mg-Al layered double hydroxide) in presence of different anions. *Cem. Concr. Res.* **2022**, *152*, No. 106674.
(38) Tarutani, N.; Honda, Y.; Hamakawa, R.; Uchikoshi, T.; Ishigaki, T. Shell-thickness control of hollow SiO_2 nanoparticles through post-treatment using sol−gel technique toward efficient water confinement. *Colloids Surf., A* **2021**, *629*, No. 127501.
(39) Liu, C.; Wang, A.; Yin, H.; Shen, Y.; Jiang, T. Preparation of nanosized hollow silica spheres from Na_2SiO_3 using Fe_3O_4 nanoparticles as templates. *Particuology* **2012**, *10* (3), 352−358.
(40) Wang, Q.; Tay, H. H.; Guo, Z.; Chen, L.; Liu, Y.; Chang, J.; Zhong, Z.; Luo, J.; Borgna, A. Morphology and composition controllable synthesis of Mg−Al−CO_3 hydrotalcites by tuning the synthesis pH and the CO_2 capture capacity. *Appl. Clay. Sci.* **2012**, *55*, 18−26.
(41) Xu, Z. P.; Stevenson, G. S.; Lu, C. Q.; Lu, G. Q.; Bartlett, P. F.; Gray, P. P. Stable suspension of layered double hydroxide nanoparticles in aqueous solution. *J. Am. Chem. Soc.* **2006**, *128* (1), 36−37.
(42) Vuong, P. M.; Thoa, T. T. K.; Nhu, P. Q.; No, N. T. H.; Ty, N. M.; Huy, D. M.; Thao, P. T.; Hang, T. T. X. Controllable synthesis of uniform MgAl-hydrotalcite nanoplates and their size-dependent on anti-corrosion properties of carbon steel. *Vietnam. J. Chem.* **2022**, *60*, 32−40.
(43) Xing, Z.; Tay, S.-W.; Ng, Y. H.; Hong, L. Porous SiO_2 hollow spheres as a solar reflective pigment for coatings. *ACS. Appl. Mater. Interfaces.* **2017**, *9* (17), 15103−15113.
(44) Iyi, N.; Matsumoto, T.; Kaneko, Y.; Kitamura, K. A novel synthetic route to layered double hydroxides using hexamethylenetetramine. *Chem. Lett.* **2004**, *33* (9), 1122−1123.
(45) Iyi, N.; Ebina, Y.; Sasaki, T. Synthesis and characterization of water-swellable LDH (layered double hydroxide) hybrids containing sulfonate-type intercalant. *J. Mater. Chem.* **2011**, *21* (22), 8085−8095.
(46) Thommes, M.; Cychosz, K. A. Physical adsorption characterization of nanoporous materials: progress and challenges. *Adsorption.* **2014**, *20* (2−3), 233−250.
(47) Son, S.; Hwang, S. H.; Kim, C.; Yun, J. Y.; Jang, J. Designed synthesis of SiO_2/TiO_2 core/shell structure as light scattering material for highly efficient dye-sensitized solar cells. *ACS. Appl. Mater. Interfaces.* **2013**, *5* (11), 4815−4820.
(48) Phattharachindanuwong, C.; Hansupalak, N.; Plank, J.; Chisti, Y. Template-assisted facile synthesis and characterization of hollow calcium silicate hydrate particles for use as reflective materials. *Mater. Res. Bull.* **2018**, *97*, 343−350.
(49) Hu, Y.; Mei, R.; An, Z.; Zhang, J. Silicon rubber/hollow glass microsphere composites: Influence of broken hollow glass microsphere on mechanical and thermal insulation property. *Compos. Sci. Technol.* **2013**, *79*, 64−69.

https://doi.org/10.1021/acsomega.3c03917
ACS Omega 2023, 8, 31399−31409